

# THE MCS INVESTIGATION: OVERVIEW OF RECENT SCIENCE RESULTS

**D. M. Kass, D. J. McCleese, W. A. Abdou, A. Kleinböhl, P. O. Hayne, T. McDunn, S. Piqueux, J. H. Shirley, J. T. Schofield, and the MCS Team, Jet Propulsion Laboratory/California Institute of Technology, Pasadena, California, USA** (*David.M.Kass@jpl.nasa.gov*).

## Instrument and Spacecraft:

Mars Climate Sounder (MCS) is a passive 9-channel radiometer on the Mars Reconnaissance Orbiter (MRO) that is optimized for atmospheric observations [McCleese *et al.*, 2007]. It uses limb staring to obtain atmospheric profiles from the surface to  $\sim$ 80 km. The instrument consists of two telescopes that are designed to be slewed in azimuth and elevation to view the martian atmosphere in limb, nadir, and on-planet geometries. Each channel consists of 21 detectors, which observe the atmosphere simultaneously. Their angular separation provides an altitude resolution of  $\sim$ 5 km (half a scale height) at the Mars limb.

MCS has 8 mid- and far-infrared channels and one visible/near-IR channel, covering 0.3 to 45  $\mu$ m (Figure 1). Three channels cover frequencies around the 15  $\mu$ m CO<sub>2</sub> absorption band (A1, A2 and A3) and are used for pressure and temperature sounding. A channel centered around 22  $\mu$ m (A5) gives information about dust opacity while a channel centered at 12  $\mu$ m (A4) covers an absorption feature of water ice. In the far-IR three channels (B1, B2, and B3) are designed to give information about surface temperature, water vapor abundance and dust and condensate opacities.

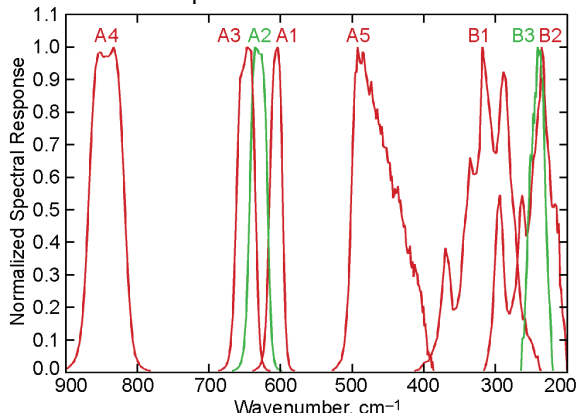


Figure 1. MCS IR spectral channels

MRO is in a sun-synchronous polar orbit [Zurek and Smrekar, 2007] and provides global observations at 3 AM and 3 PM. The polar MRO orbit covers all longitudes in 13 orbits (each separated by  $\sim$ 27°) over 24 hours 20 minutes. Each day, the ground track "walks"  $\sim$ 5° to the east.

## MCS Profile Retrievals:

The MCS retrieval algorithm [Kleinböhl *et al.*, 2009, and Kleinböhl *et al.*, 2011] produces vertical

profiles of temperature, dust and water ice extinction versus pressure. It also produces surface brightness temperatures. The retrievals are based on a modified Chahine method [Chahine, 1972]. This is an iterative technique that simultaneously solves for all fields by minimizing the radiance residuals. The algorithm uses both limb observations and (where available) nearby on-planet or nadir observations. The on-planet observations are used for the surface temperature retrieval and to retrieve the temperature in the lower atmosphere when the limb is too opaque due to aerosols.

The gas radiative transfer is performed using the Curtis-Godson approximation with precalculated transmissions for each channel. Aerosol radiative transfer is performed using both absorption and single scattering. The dust and water ice properties are determined with Mie calculations using a gamma distribution with an  $r_{\text{eff}} = 1.06 \mu\text{m}$  for dust and an  $r_{\text{eff}} = 1.4 \mu\text{m}$  for water ice. The radiative transfer assumes a spherically symmetric atmosphere.

In some cases, the atmosphere is too opaque along the limb path at  $\sim$ 25 km for the pressure retrieval to succeed. This is due to the existence of thick aerosol (dust or water ice). The pressure retrieval can also fail due to very sharp horizontal atmospheric gradients. In either case, a retrieval using a climatological surface pressure will be performed.

In cases where there are no on-planet observations, the surface temperature cannot be retrieved. A climatological surface temperature is used to characterize the upwelling radiation flux that is used in aerosol scattering radiative transfer.

All retrievals are evaluated for success based on the radiance residuals. (The extent to which the retrieved profile converges on the measured radiances.) In some cases, the entire profile needs to be rejected. In other cases, the profile needs to be truncated above the surface. This is due to either poor convergence at low altitudes or opaque aerosol (usually an extinction greater than about  $4 \times 10^{-3} \text{ km}^{-1}$ ).

## Public Archive:

The retrieved MCS profiles for the entire mission are publicly archived at the PDS Atmospheres node ([http://atmos.pds.nasa.gov/data\\_and\\_services/atmospheres\\_data/Mars/Mars.html](http://atmos.pds.nasa.gov/data_and_services/atmospheres_data/Mars/Mars.html)). PDS designates the current version of the profiles as v2. Profiles are delivered to the PDS on a regular schedule every three months. Each delivery covers three months of data.

### Ongoing Retrieval Improvements:

The MCS team is continually improving the retrieval algorithm. This involves the development of research algorithms that are used on specific periods of observations. Those that are successful and well tested are folded back into the operational retrieval algorithm to produce enhanced retrievals for the community.

Several modifications to the MCS retrieval algorithm have been developed that facilitate profile retrievals in high-dust conditions. These modifications are particularly relevant for retrievals during the 2007 dust storm as MCS did not perform on-planet measurements during this time. These include the following key modifications:

- The range of aerosol retrievals has been extended to higher altitudes.
- A correction to the surface temperature climatology has been developed. The climatology is based on non-duststorm conditions. In conditions of a global dust storm, surface temperatures tend to be lower than prescribed in the climatology. Taking this into account using an adaptive value based on retrieved atmospheric opacity leads to improved fits to the radiances measured by MCS and improves the retrieval success rate.

The team is developing a 2-D radiative transfer scheme and retrieval algorithm. This allows the retrieval algorithm to handle horizontal gradients in the atmosphere. This can be important in regions with sharp gradients due to the ~250 km horizontal weighting functions for the MCS limb observations.

Retrievals of CO<sub>2</sub> ice are also in development for the winter polar regions (see the Hayne et al., abstract at this conference). CO<sub>2</sub> ice extinction is retrieved from limb measurements using large ( $r_{\text{eff}} = 32 \mu\text{m}$ ) CO<sub>2</sub> ice particles. In these regions, MCS radiances regularly show characteristic signs of CO<sub>2</sub> ice clouds [Hayne et al., 2012].

### MCS Mission:

The MCS observations cover almost four complete Mars Years (Figure 2). MCS has been collecting data since around Ls 110° of MY 28 (September, 2006). Initially, MCS performed full in-track limb/nadir and polar scanning. Due to an anomaly in one of the actuators the instrument took measurements in limb staring geometry from Ls 180° to 260° of that year. During this time (yellow), the quality of the calibration is reduced. In addition, the vertical coverage is somewhat limited.

Since then, the instrument has performed limb tracking and full calibration activities. For most of the time, on-planet observations have also been acquired. These are off-nadir with an airmass factor of ~2.5.

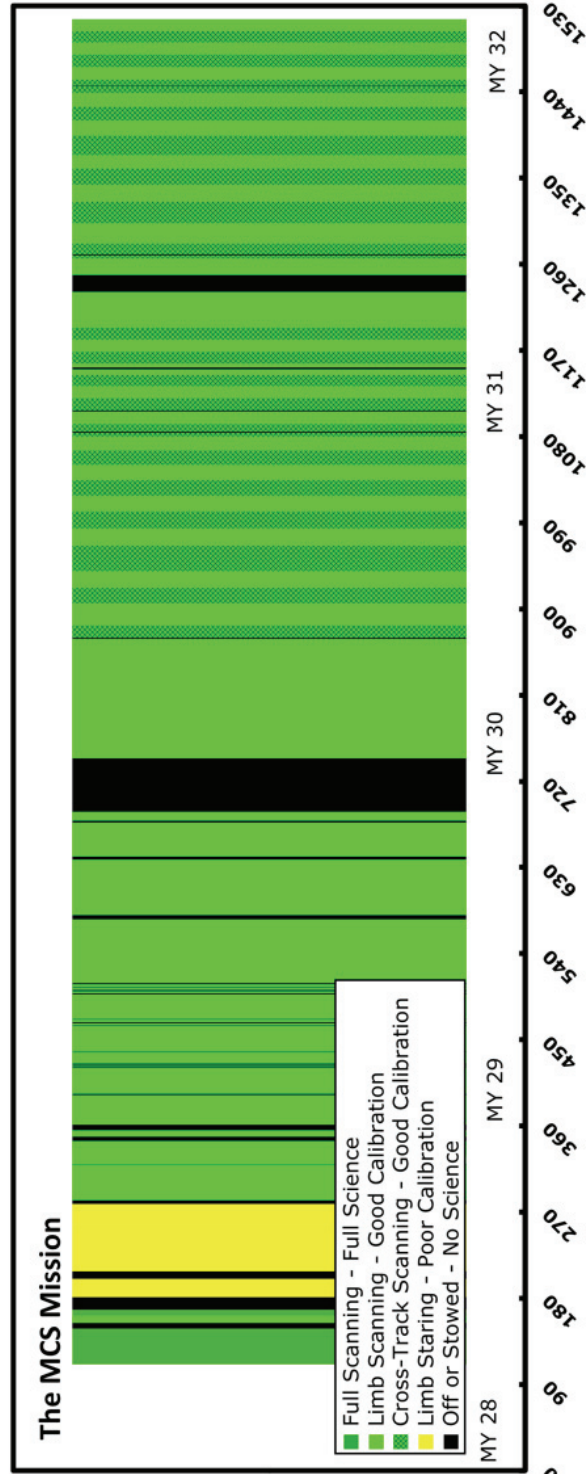


Figure 2. MCS Mission Timeline. Ls is continuous starting with the beginning of MY 28.

Starting around Ls 150 of MY 30 (September 2010), the instrument has performed regular time-of-day campaigns (shown as crosshatched areas in Fig. 2). The additional local times are obtained by having the instrument perform cross-track observations (views of the atmosphere perpendicular to the orbit track). During each time-of-day campaign, the horizontal spacing along the track (at 3 AM/3 PM) is reduced and observations are acquired at additional

local times. The additional local times range from  $\pm 1.5$  hours at the equator to most of the diurnal cycle in the polar regions. Each campaign lasts four weeks and alternate with four weeklong periods of regular (in-track) scanning.

### Latitudinal and Vertical Structure of Temperature and Dust During the 2007 Global Dust Storm:

The global dust storm of Mars Year 28 started in the second half of June 2007. Dust was lifted into the middle atmosphere and the atmospheric dust loading increased on a planet encircling scale. By mid-July 2007 the dust storm was in full force, although dust was still not distributed homogeneously around the planet.

The top panels of Fig. 3 show a transect of retrievals of temperature and dust extinction along the dayside part of an orbit on July 12, 2007. Retrievals in high-dust conditions are possible between altitudes of 30-40 km, below which the atmosphere is nearly opaque in the limb, and  $\sim 80$  km, which corresponds to the top of the MCS detector array. High dust opacities are found from the south pole to the northern mid-latitudes. Only beyond  $\sim 50^\circ\text{N}$  the dust opacity decreases significantly.

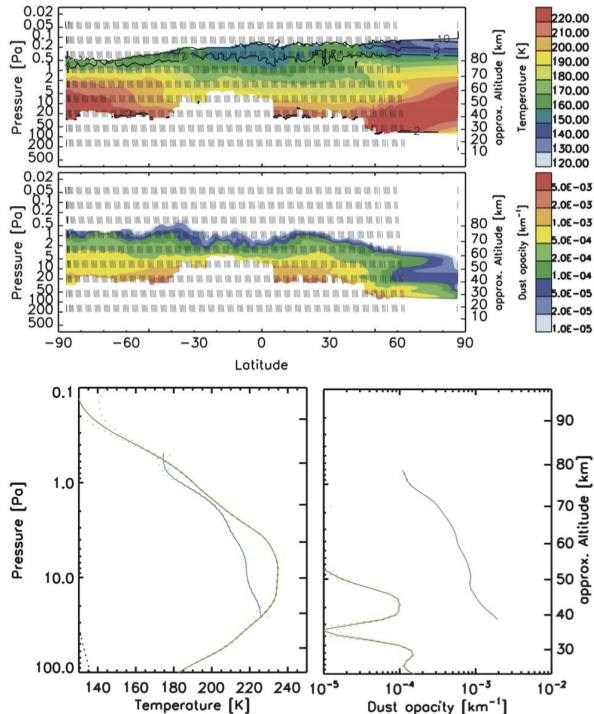


*Figure 3: Temperature (top panel) and dust opacity (middle panel) vs. pressure as measured by MCS on the dayside part of one orbit on July 12, 2007 ( $L_s = 274.7^\circ$ , MY 28). The bottom panel shows individual temperature (bottom left) and dust (bottom right) profiles representative for southern mid-latitudes ( $\sim 55^\circ\text{S}$ , blue) and northern high latitudes ( $\sim 85^\circ\text{N}$ , brown).*

The bottom panels of Fig. 3 show examples of

profiles retrieved along this orbit. In the southern high latitudes dust is nearly homogeneously mixed throughout the altitude range in which retrievals can be performed. Even at 80 km the retrieved dust extinction is still  $\sim 10^{-4} \text{ km}^{-1}$ , and no fall-off of the dust profile below homogeneously mixed is discernible. Temperatures in these conditions range from about 220 K at 40 km to 180 K at 80 km. The maximum altitudes at which significant dust opacities are observed seem to exceed the maximum altitudes at which TES limb observations detected dust in the global dust storm of 2001 [Clancy *et al.*, 2010]. Around the north pole the observed dust opacity is significantly lower than elsewhere on the planet. At  $\sim 240$  K this is the region where the highest temperatures in the middle atmosphere are observed. The absence of high dust opacities and solar heating suggests that the temperatures in this region result from adiabatic heating in the downwelling part of the overturning meridional circulation, which is strongly enhanced in global dust storm conditions.

### Seasonal Polar Cap Edge Tracking:

The seasonal caps are a large and dynamic reservoir of  $\text{CO}_2$  on Mars. Their growth and retreat in response to the seasonal change of solar illumination has been monitored for  $\sim 150$  years and has shown localized inter-annual variability mostly attributed to the effect of regional and global dust storms. However, systematic regional-scale studies of the inter-annual variability of the extent of the caps have been complicated by the poor illumination conditions of the polar regions, the frequent presence of clouds/hazes obscuring the surface, and the difficulty in differentiating  $\text{H}_2\text{O}$  from  $\text{CO}_2$  ices. MCS measurements of the surface temperature through channel B1 ( $\sim 32\mu\text{m}$ , Fig. 1) are well suited to map and track the edges of the caps: brightness temperatures 1) are diagnostic of polar surface materials, 2) can be acquired under all illumination conditions, and 3) are minimally distorted by atmospheric contributions. In addition, MCS channel B1 spectral response can be emulated using TES spectra to establish a long-term record of the seasonal cap edge behaviors.

Eight Mars Years of cap tracking (Figure 4) show for the North that, inter-annual variability of the cap surface area is  $\sim 5-15 \text{ } 10^5 \text{ km}^2$  out of a maximum extent of almost  $2 \text{ } 10^7 \text{ km}^2$ . The recession does not display pauses and accelerations as suggested by visible observations. The shape of the northern cap is partially controlled by the regional topography (Tempe Terra and Alba Patera). The MY25 dust storm does not have an effect on the surface area and retreat rate of the cap, but the MY28 dust storm clearly sped it up compared to other years (Figure 5). During clear years, the inter-annual repeatability is very high in most regions. For the South, greater inter-annual variability is observed, especially near the time of maximum cap extent ( $L_s \sim 90$ ) with variability concentrated in Hellas, and when the basal

venting of the cap deposits significant amounts of particulates on top of the ice ( $190^\circ < Ls < 220^\circ$ ) in the Cryptic Region. The MY25 dust storm clearly accelerated the recession of the South seasonal cap (the seasonal cap had essentially sublimated at the time of the MY 28 dust storm). The MCS team is currently generating climatological cap edge maps typical of cap growth and recession for clear years.

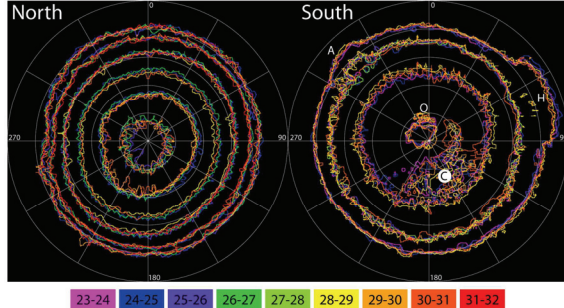


*Figure 4. Inter-annual comparison of North and South seasonal cap edges at selected seasons. Cap edges are color-coded by MY cycles. North seasonal cap edges at  $Ls = 285^\circ, 315^\circ, 345^\circ, 15^\circ, 45^\circ$ , and  $75^\circ$ . South seasonal cap edges at  $Ls = 105^\circ, 165^\circ, 215^\circ$  and  $295^\circ$ . Letters indicate regions of interest: A refers to Argyre, C to the Cryptic Region, H to Hellas, and O to the water ice outlier. Missing cap edges are due to absence of data or low quality data. Cap edge for MY25 at  $Ls = 215^\circ$  not shown for clarity. Latitude grid every  $10^\circ$ , longitude grid every  $30^\circ$ , with markers every  $90^\circ$  (East longitude).*

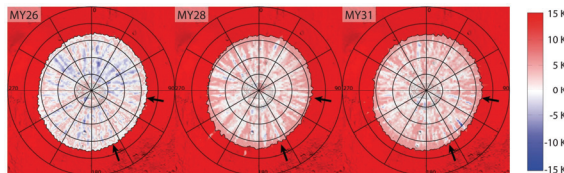


*Figure 5. North seasonal cap edges (black line) on MY28 at  $330^\circ < Ls < 340^\circ$  following a global dust storm (Center) compared to cap edges determined at the same season on two typical other years (MY26, Left; MY31, Right, selected based on data quality and distribution). Arrows indicate regions of most accelerated retreat on MY28 compared to other years. Latitude grid every  $10^\circ$ , longitude grid every  $30^\circ$ , with markers every  $90^\circ$  (East longitude). Background is a MOLA shaded relief map. Colors indicate the amplitude of diurnal temperature variations.*

#### Winter Polar CO<sub>2</sub> Ice Retrievals:

The 2-D retrieval and the retrieval of CO<sub>2</sub> ice in the winter polar region are complementary. The sharp horizontal temperature gradients and complex temperature structure within the winter polar vortex are difficult to retrieve with a spherically symmetric assumption. The team has been exploring the relationships between the temperature structure and the CO<sub>2</sub> ice clouds using the combination of the 2-D retrievals and the CO<sub>2</sub> ice retrieval.

Figures 6 and 7 show the northern winter polar

region. The temperature field above  $\sim 30$  km shows the dynamical temperature increase due to the downwelling atmosphere over the pole [McCleanse *et al.*, 2008]. Below this are the inner regions of the polar vortex. The regions with temperatures below the CO<sub>2</sub> ice condensation temperature are outlined in black.

When the standard retrieval is used (Figure 6), the ice and condensation temperature are poorly aligned. However, when the 2-D retrieval is used for the temperature field, the two are much better aligned (Figure 7). There is also a more complex temperature structure within the polar region. The region of cold temperatures now include most of the regions with CO<sub>2</sub> ice. Apart from the interesting region to the left of the pole, most of the regions below the condensation temperature contain clouds. The remaining lack of alignment may be due to the 1-D nature of the CO<sub>2</sub> retrieval.

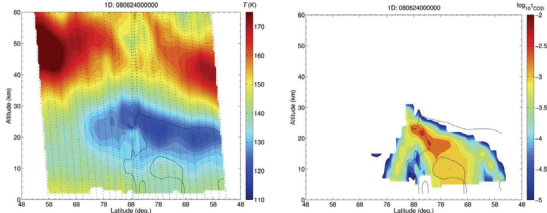


*Figure 6. Retrieved temperatures and CO<sub>2</sub> ice in the northern polar region at  $Ls = 90^\circ$ . The left panel contains the retrieved temperatures along a single orbit across the polar region. The dotted lines show the locations of individual retrievals. The right panel contains the retrieved CO<sub>2</sub> extinction ( $km^{-1}$ ) at  $463\text{ cm}^{-1}$  (or  $21.6\text{ }\mu\text{m}$ ) along the same orbit on a log scale.*

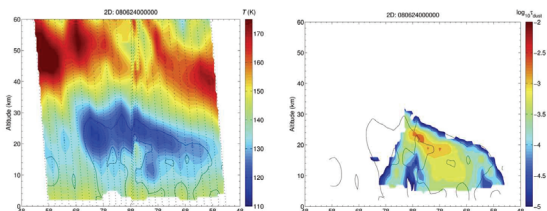


*Figure 7. The same as Figure 6, but using the 2-D retrieval algorithm.*

**References:** Chahine (1972), *J. Atmos. Sci.*, 29; Clancy *et al.* (2010), *Icarus*, 207; Hayne *et al.* (2012), *JGR*, 117, doi: 10.1029/2011JE004040; Kleinböhl *et al.* (2009), *JGR* 114, E10006, doi: 10.1029/2009JE003358; Kleinböhl *et al.* (2011), *JQRST*, 112, 1568-1580; McCleese *et al.* (2007), *JGR*, 112, E05S06 doi: 10.1029/2006JE002790; McCleese *et al.* (2008), *Nat. Geosci.*, 1, doi: 10.1038/ngeo332; Zurek and Smrekar (2007), *JGR*, 112, E05S01, doi: 10.1029/2006JE002701.

**Acknowledgement:** This work was carried out at the Jet Propulsion Laboratory, California Institute of Technology under a contract with the National Aeronautics and Space Administration.